3-D Numerical Simulations of Biofilm Flows

Chen Chen[1], Mingming Ren[1,2], Ashok Srinivansan[3] and Qi Wang[*,1]

[1] *Department of Mathematics, University of South Carolina, Columbia, SC 29063, USA.*

[2] *Beijing Computational Science Research Center, Beijing, 100084, China.*

[3] *Department of Computer Science, Florida State University, Tallahassee, FL 32302, USA.*

Abstract. We study the biofilm-flow interaction resulting in biofilm growth and deformation in a water channel in a 3-D setting using the phase field model developed recently [28, 29]. In this biofilm model, the biofilm made up of the EPS, bacteria and solvent is tracked using a biofilm volume fraction which vanishes outside the biofilm region. The interface between the biofilm and the solvent is marked by the zero level surface of the volume fraction measured from the biofilm to the solvent. The growth of the biofilm and the solvent-biofilm interaction with the top nutrient feeding condition is simulated in the viscous regime (growth regime) of the biofilm-solvent mixture flow. In quiescent flows, the model predicts growth patterns consistent with experimental findings for single or multiple adjacent biofilm colonies, in which the known mushroom shape growth pattern is obtained. Shear induced deformation in biofilms is simulated in a shear cell, providing a viable numerical evidence for using simulation tool to study biofilm growth and interaction dynamics in aqueous environment.

1. Introduction

Biofilms are ubiquitous in nature, water filtering devices, plumbing pipes, medical implants, and dentistry etc. Biofilms form when bacteria adhere to surfaces in moist environments by excreting a slimy, glue-like substance. Sites for biofilm formation include all kinds of surfaces: natural materials above and below ground, metals, plastics, medical implant materials, teeth, plants and body tissues. Wherever you find a combination of moisture, bacteria, nutrients and a surface, you are likely to find biofilms.

A biofilm community can be formed by a single bacterial species, but in nature biofilms almost always consist of rich mixtures of many species of bacteria, as well as fungi, algae, yeasts, protozoa, other microorganisms, debris and corrosion products. Biofilms are

---

*Corresponding author. *Email address:* `wangq@mailbox.sc.edu` (Q. Wang)

held together by sugary molecular strands, collectively termed "extracellular polymeric substances" or "EPS". The bacterial cells produce EPS; and they are held together by these strands, allowing them to develop complex, three-dimensional, resilient, attached communities. Biofilms cost the U.S. literally billions of dollars every year in energy losses, equipment damage, product contamination and medical infections. But biofilms can also offer huge potential for bio-remediating hazardous waste sites, bio-filtering municipal and industrial water and waste water, forming bio-barriers to protect soil and ground water from contamination, and as well as heap leaching [7, 11, 13].

The formation of biofilm colonies is a complex biological and transport phenomenon. The arrival of the EPS producing biological cells react to the environment and communication among themselves to build their biofilm community. In this process, a supporting substrate, sufficient number of EPS producing cells, sufficient delivery and supply of nutrient materials, and cellular communication dictate how the community is built. Experimentally, one notices that the gene expression of the biofilm is quite distinct from the gene expression of a platonic cell and then turn to suspect that the biofilm community not only protect the encased bacterial or other biological cells, but also alter their cellular behavior. The viable explanation is that there exist active cellular communication channels or signaling pathways to alter the cellular response and function in the biofilm community. Quorum sensing is a phenomenon identified with the microorganism like the biofilm in which certain cellular behavior is turned on or off depending on the baseline population in the biofilm community. On the other hand, for the living organisms, supply of nutrients is vital to their survival and development.

Biofilms consist of a large amount of water in addition to bacteria, EPS, and various nutrients. The EPS exists in the form of polymeric networks allowing sustances of small molecules such as water and nutrients to permeate as well as large bacterial cells to migrate. So, the biofilm collectively behave like a gel. It is a challenge to model the live microorganism in biofilms and their transient growth, molecular signaling and transport behavior altogether. There have been various multi-fluid models proposed to predict growth behavior of biofilms, in which the biofilm community is modeled either using hybrid discrete and differential models [20–24] or mechanistically using continuum models as a biological gel [6, 14–19, 27]. However, it becomes tricky when one uses the biogel models to study dynamics of biofilms in another fluid in a geometry where an inflow and outflow boundary condition need to be specified since the velocity boundary conditions for the multi-fluid model are hard to define. When constitutive equations are also present for viscoelastic components, there could also be boundary conditions for the extra elastic stress tensor corresponding to the components, creating another layer of complication for the use of the models.

The fundamental assumption in the multi-fluid models is that the momentum of each fluid component must be conserved so that the individual velocity for each fluid is employed. In practice, it's the average velocity of the mixture that can be measured in various fluid devices. Often, it is the mass average velocity chosen as the one to be measured. With the notation of the average velocity, each individual velocity is decomposed into a sum of the average one and an excessive one. The hydrodynamical identity of the excessive veloc-

ity depends exclusively on the momentum transport equation of each fluid component. It can be viewed as a mixing velocity in the frame moving with the average velocity. Parallel to the multifluid formulation of hydrodynamical theories for fluid mixture, there is another formalism termed one fluid multi-component in which an average velocity is designated as the primary hydrodynamic variable and the excessive velocity relative to the average one is dictated by the fluid system potential. For flow-biofilm interaction, a single fluid multicomponent model would be more appropriate and efficient since it does not inflict the ambiquity on the inflow and/or outflow boundary condition.

Recently, we developed a phase-field based hydrodynamic theory for mixtures of biofilm and solvent flows using the one fluid multi-component formulation [1, 28, 29]. The model captures the long wave growth phenomenon exhibited in biofilm growth. The preliminary study on 1-D and 2-D biofilm growth shows promising results for the theory to be used in studying dynamics of the biofilm growth and biofilm interaction with the ambient solvent. The fundamental difference between this formulation and the multi-fluid formulation is the excessive velocity. In the multi-fluid theory, the excessive velocity is determined by the momentum balance for each individual fluid component; whereas, in this model, the excessive velocity is dictated by the system energy. Namely, we stipulate that in this theory the mixing between different fluid component relative to the average velocity is given by a nonequilibrium thermodynamical process governed by the system potential.

In this paper, we expand our investigation of the biofilm dynamics in 3 space dimensions using the phase field theory in the growth regime, where the collective behavior of the fluid mixture is viscous or more precisely extended Newtonian. We will present the study on 3-D biofilm growth in quiescent flows and investigate how a shear flow interacts with the grown biofilm colony.

2. Mathematical Model

We first recall the mathematical model developed for the mixture of biofilms and solvent in [28]. Let $\mathbf{v}$ denote the average velocity, p the hydrostatic pressure, ϕ_n and ϕ_s the volume fraction of the effective polymer network and the effective solvent respectively, and c the nutrient concentration. The phase field theory for the mixture of biofilms and solvent consists of four sets of equations.

Momentum and continuity equation
We assume the average velocity is solenoidal and the linear and angular momentum of the system is conserved [2, 8]:

$$\nabla \cdot \mathbf{v} = 0,$$
$$\rho \frac{d\mathbf{v}}{dt} = \nabla \cdot (\phi_n \tau_n + \phi_s \tau_s) - \left[\nabla p + \gamma_1 k_B T \nabla \cdot (\nabla \phi_n \nabla \phi_n) \right], \qquad (2.1)$$

where $\rho = \phi_n \rho_n + \phi_s \rho_s$ is the effective density for the mixture, ρ_n and ρ_s are the density for the effective polymer network and the solvent, respectively, τ_n and τ_s are the extra stress for the polymer network and the solvent, respectively, k_B is the Boltzmann constant,

T is the temperature, γ_1 is a parameter measures the strength of the conformational entropy and γ_2 is the strength of the bulk mixing free energy in the extended Flory-Huggin's mixing free energy density defined by [9, 10, 12, 26]

$$f = \frac{\gamma_1}{2}kT \left\| \nabla \phi_n \right\|^2 + \gamma_2 kT \left[\frac{\phi_n}{N} \ln(\phi_n + \epsilon) + (1 - \phi_n)\ln(1 - \phi_n) + \chi \phi_n (1 - \phi_n) \right]. \quad (2.2)$$

Here γ_2 is proportional to the reciprocal of the volume of the solvent molecule, N is the polymerization index for the polymer strand in the EPS network, χ is the mixing parameter, and ϵ is a small dimensionless parameter to regularize the potential in the pure solvent region. In this paper $\epsilon = 10^{-12}$ is used. For this fluid mixture, we also assume it is incompressible in the sense of

$$\phi_s + \phi_n = 1. \quad (2.3)$$

The incompressibility is an approximation to the mixture system. It is valid when the density deviation between the two effective components in the mixture is small. For biofilms, the density deviation between the effective polymer network and the solvent is not very large. So, this is a valid approximation.

Transport equation for the volume fraction of the effective polymer network

We adopt the Cahn-Hilliard equation for the transport of the volume fraction of effective polymers:

$$v \frac{\partial \phi_n}{\partial t} + \nabla \cdot (\phi_n \mathbf{v}) = \nabla \cdot \left[\lambda \phi_n \nabla \frac{\delta f}{\delta \phi_n} \right] + g_n, \qquad \text{MCH-model}, \quad (2.4)$$

where λ is the mobility parameter and the polymer network production rate is given by

$$g_n = \mu \phi_n \frac{c}{K_c + c}, \quad (2.5)$$

μ is the maximum production rate, K_c is the half-saturation constant. The prefix M indicates the transport equation is a modified or singular Cahn-Hilliard equation with a polymer volume fraction dependent mobility [3, 5]. This is the more relevant mobility definition for the mixture of a biofilm and solvent since the Cahn-Hilliard equation should be trivial in the pure solvent region, i.e., there is no polymer network to be transported therein.

Constitutive equations

There are multiple time scales in the biofilm model we developed. The polymer relaxation time scale is measured in the range of seconds or minutes while the biofilm growth time scale is normally measured in hours and days. The biofilm behaves like a Newtonian or viscous fluid in large time scale when the elastic stress relaxes, which turns out to be common in biofilm growth. In the regime of this time scale, the constitutive equation is

therefore given by the viscous constitutive equation for the stress contribution from both the effective polymer network and the solvent:

$$\tau_n = 2\eta_n \mathbf{D}, \quad \tau_s = 2\eta_s \mathbf{D}, \quad \text{VA-model},$$
$$\tau_n = 2\eta_n \mathbf{D}_n, \quad \tau_s = 2\eta_s \mathbf{D}_s, \quad \text{VN-model}. \tag{2.6}$$

Here we present two versions of the constitutive equations. One uses the average velocity to compute the rate of strain while the other uses the effective polymer velocity. Presumably the latter is more accurate. But, in many cases, the former is convenient and also a good approximation. The polymer network velocity is defined by

$$\mathbf{v}_n = \mathbf{v} - \lambda \nabla \frac{\delta f}{\delta \phi_n}. \tag{2.7}$$

The solvent velocity is defined by

$$\mathbf{v}_s = \mathbf{v} + \frac{\lambda \phi_n}{\phi_s} \nabla \frac{\delta f}{\delta \phi_n}. \tag{2.8}$$

The polymer velocity and the solvent velocity coincides with the average velocity outside the biofilm region. The rate of strain tensor and the vorticity tensor with respect to the average velocity are given by

$$\mathbf{D} = \frac{1}{2}[\nabla \mathbf{v} + \nabla \mathbf{v}^T], \quad \mathbf{W} = \frac{1}{2}[\nabla \mathbf{v} - \nabla \mathbf{v}^T].$$

The corresponding ones with respect to the network velocity are defined analogously

$$\mathbf{D}_n = \frac{1}{2}[\nabla \mathbf{v}_n + \nabla \mathbf{v}_n^T], \quad \mathbf{W}_n = \frac{1}{2}[\nabla \mathbf{v}_n - \nabla \mathbf{v}_n^T].$$

In small to intermediate time scales, the EPS molecular relaxation time is comparable to the characteristic time scale of the fluid mixture system, the EPS contribution is viscoelastic and can be approximated by the following Johnson-Segalman model [2, 12]:

$$\frac{\partial \tau_n}{\partial t} + \mathbf{v} \cdot \nabla \tau_n - \mathbf{W} \cdot \tau_n + \tau_n \cdot \mathbf{W} - a[\mathbf{D} \cdot \tau_n + \tau_n \cdot \mathbf{D}] + \frac{\tau_n}{\lambda_1} = \frac{2\eta_n}{\lambda_1}\mathbf{D}, \qquad \text{JSA-model}$$
$$\tau_s = 2\eta_s \mathbf{D},$$
$$\frac{\partial \tau_n}{\partial t} + \mathbf{v}_n \cdot \nabla \tau_n - \mathbf{W}_n \cdot \tau_n + \tau_n \cdot \mathbf{W}_n - a[\mathbf{D}_n \cdot \tau_n + \tau_n \cdot \mathbf{D}_n] + \frac{\tau_n}{\lambda_1} = \frac{2\eta_n}{\lambda_1}\mathbf{D}_n, \qquad \text{JSN-model}$$
$$\tau_s = 2\eta_s \mathbf{D}_s, \tag{2.9}$$

where η_n and η_s are the viscosity for polymer network and solvent respectively, and the infinite relaxation time limit $\lambda_1 \to \infty$ yields the pure elastic theory. In the other limit $\lambda_1 \to 0$, the viscous constitutive equation is recovered. The suffix A and N in the above equations indicate the average or network velocity are used in convection, respectively.

Transport equation for nutrient substrates

The transport equation for the nutrient is given by the transport of the effective nutrient that is carried in the solvent:

$$\frac{\partial}{\partial t}(\phi_s c) + \nabla \cdot (c\mathbf{v}_s \phi_s - D_s \phi_s \nabla c) = -g_c, \qquad (2.10)$$

where c is the nutrient concentration and the nutrient consumption rate is given by

$$g_c = \phi_n \frac{Ac}{k_1 + c}, \qquad (2.11)$$

A is a consumption rate constant, k_1 is a half saturation rate, and D_s is the diffusion constant for the nutrient substrate.

We investigate the dynamics of the biofilm in 3 space dimensions: $(x, y, z) \in \Omega = [0, L] \times [0, H] \times [0, K]$, where H, K, L are positive constants. We consider the biofilm solvent mixture in a shear cell. We impose periodic boundary conditions in the x and z direction and physical boundary conditions in y direction: no-flux boundary conditions for the volume fraction of effective polymer and nutrient substrate concentration (at $y = 0$ only),

$$[c\mathbf{v}_s \phi_s - D_s \phi_s \nabla c] \cdot \mathbf{n}|_{y=0} = 0,$$

$$\nabla \phi_n \cdot \mathbf{n}|_{y=0,H} = 0,$$

$$\left[\mathbf{v}\phi_n - \Lambda \nabla \frac{\delta f}{\delta \phi_n}\right] \cdot \mathbf{n}|_{y=0,H} = 0,$$

$$\mathbf{v}|_{y=0} = 0, \quad \mathbf{v}|_{y=H} = \mathbf{v}_0. \qquad (2.12)$$

Here $\mathbf{v}_0$ is the velocity for the top boundary which moves at a speed in the shear flow simulation. The top feeding boundary condition is given for c:

$$c|_{y=H} = c^* \qquad (2.13)$$

in place of the zero-flux condition there.

3. Nondimensionalization

We use a characteristic time scale t_0 and length scale h to nondimensionalize the variables

$$\tilde{t} = \frac{t}{t_0}, \quad \tilde{\mathbf{x}} = \frac{\mathbf{x}}{h}, \quad \tilde{\mathbf{v}} = \frac{\mathbf{v}t_0}{h}, \quad \tilde{p} = \frac{pt_0^2}{\rho_0 h^2}, \quad \tilde{c} = \frac{c}{c_0}, \qquad (3.1)$$

where c_0 is a characteristic substrate concentration. The length scale h is determined by the computational geometry while the time scale is done by either the growth time scale

of the biofilm or the flow induced time scale. After nondimensionalization, the following dimensionless parameters arise

$$\Lambda = \frac{\lambda \rho_0}{t_0}, \quad \Gamma_1 = \frac{\gamma_1 k T t_0^2}{\rho_0 h^4}, \quad \Gamma_2 = \frac{\gamma_2 k T t_0^2}{\rho_0 h^2}, \quad Re_s = \frac{\rho_0 h^2}{\eta_s t_0}, \quad Re_n = \frac{\rho_0 h^2}{\eta_n t_0}, \quad \tilde{D}_s = \frac{D_s t_0}{h^2},$$

$$\tilde{\rho} = \phi_s \frac{\rho_s}{\rho_0} + \phi_n \frac{\rho_n}{\rho_0}, \quad \tilde{A} = A t_0, \quad \tilde{\mu} = \mu t_0, \quad \tilde{K}_c = \frac{K_c}{c_0}, \quad \tilde{K}_1 = \frac{k_1}{c_0}, \tag{3.2}$$

where Re_s and Re_n are the Reynolds number for the effective solvent and the effective polymer, respectively, ρ_0 is an averaged density, $\tilde{\Lambda}$ is the dimensionless mobility parameter. In this paper, we use the extended Newtonian model for the polymeric stress tensor and the MCH equation for the effective polymer volume fraction. For simplicity, we drop the ~ on the dimensionless variables and the parameters and the system of governing equations for extended Newtonian biofilm in these dimensionless variables are given by

$$\nabla \cdot (\mathbf{v}) = 0,$$

$$\rho \frac{d\mathbf{v}}{dt} = \nabla \cdot (\phi_n \tau_n + \phi_s \tau_s) - [\nabla p + \Gamma_1 \nabla \cdot (\nabla \phi_n \nabla \phi_n)],$$

$$\frac{\partial}{\partial t}(\phi_s c) + \nabla \cdot (c \mathbf{v}_s \phi_s - D_s \phi_s \nabla c) = -g_c,$$

$$\frac{\partial \phi_n}{\partial t} + \nabla \cdot \left(\phi_n \mathbf{v}\right) = \nabla \cdot \left(\Lambda \phi_n \nabla \frac{\delta f}{\delta \phi_n}\right) + g_n, \tag{3.3}$$

where

$$\tau_n = \frac{2}{Re_n}\mathbf{D}, \quad \tau_s = \frac{2}{Re_s}\mathbf{D}, \quad g_c = A\frac{\phi_n c}{K_1 + c}, \quad g_n = \mu \phi_n \frac{c}{K_c + c}.$$

The mixing free energy density is now given by

$$f = \frac{\Gamma_1}{2} \left\|\nabla \phi_n\right\|^2 + \Gamma_2 \left[\frac{\phi_n}{N} \ln \phi_n + (1 - \phi_n)\ln(1 - \phi_n) + \chi \phi_n (1 - \phi_n)\right]. \tag{3.4}$$

We remark that the solenoidal condition on the average velocity is assumed to approximate the mass conservation. This is valid only when the density variation between the solvent and the effective polymer is not significant. The viscosity variation from the biofilm to the pure solvent can be very significant in the fluid mixture though, which is adopted in the simulation discussed next.

4. Numerical Schemes

We use the finite difference method to solve the coupled flow, phase field, and nutrient concentration transport equation. We solve the coupled momentum transport equation and the continuity equation using a Gauge-Uzawa scheme [25]. We denote

$$\mathbf{R} = -\nabla \cdot (\Gamma_1 \nabla \phi_n \nabla \phi_n) + \nabla \cdot \left(\phi_n \tau_n + \phi_s \tau_s - \frac{2}{Re_a}\mathbf{D}\right), \tag{4.1}$$

where Re_a is an averaged Reynolds number whose choice will be discussed later.

The momentum transport equation is rewritten as

$$\rho\left(\frac{\partial}{\partial t}\mathbf{v} + \mathbf{v}\cdot\nabla\mathbf{v}\right) = -\nabla p + \frac{1}{Re_a}\nabla^2\mathbf{v} + \mathbf{R}. \tag{4.2}$$

We calculate $\mathbf{v}$ and the pressure in three steps. We present the scheme for the case of periodic boundary conditions in the x and z direction and physical one in the y direction in the following. For simplicity, the second order extrapolation of any function f is denoted by $\overline{f}^{n+1} = 2f^n - f^{n-1}$.

Step 1:

$$\begin{cases} \rho^{n+1}\left[\dfrac{\mathbf{u}^{n+1}-\mathbf{v}^n}{\Delta t}\right] + \rho^{n+1}\overline{\mathbf{v}}^{n+1}\cdot\nabla\mathbf{u}^{n+1} + \dfrac{1}{Re_a}[\nabla s^n - \nabla^2\mathbf{u}^{n+1}] = \overline{\mathbf{R}}^{n+1}, \\ \mathbf{u}^{n+1}|_{y=0} = 0, \quad \mathbf{u}^{n+1}|_{y=H} = \mathbf{v}_0. \end{cases} \tag{4.3}$$

Step 2: We implement the projection step by solving a Poisson equation with the Neumann boundary condition:

$$\begin{cases} -\nabla\cdot\left(\dfrac{1}{\rho^{n+1}}\nabla\psi^{n+1}\right) = \nabla\cdot\mathbf{u}^{n+1}, \\ \dfrac{\partial\psi^{n+1}}{\partial n}\Big|_{y=0,H} = 0. \end{cases} \tag{4.4}$$

Step 3: We correct the velocity, pressure and the auxiliary variable s.

$$\begin{cases} \mathbf{v}^{n+1} = \mathbf{u}^{n+1} + \dfrac{1}{\rho^{n+1}}\nabla\psi^{n+1}, \\ s^{n+1} = s^n - \nabla\cdot\mathbf{u}^{n+1}, \\ p^{n+1} = -\dfrac{\psi^{n+1}}{\Delta t} + \dfrac{1}{Re_a}s^{n+1}. \end{cases} \tag{4.5}$$

The phase field equation for the polymer volume fraction ϕ_n is discretized by

$$\frac{3\phi_n^{n+1} - 4\phi_n^n + \phi_n^{n-1}}{2\Delta t} + \mathbf{v}^{n+1}\cdot\nabla\phi_n^{n+1} = g_n^{n+1} + \Lambda\nabla\cdot[\overline{\phi_n}^{n+1}\nabla(-\Gamma_1\nabla^2\phi_n^{n+1} - 2\Gamma_2\chi\phi_n^n)]$$
$$+ \Lambda\Gamma_2\nabla\cdot\left(\left(\frac{1}{N} + \frac{\overline{\phi_n}^{n+1}}{(1-\phi_n)^{n+1}}\right)\nabla\phi_n^{n+1}\right). \tag{4.6}$$

The substrate concentration transport equation is discretized by

$$\frac{3\phi_s^{n+1}c^{n+1} - 4\phi_s^n c^n + \phi_s^{n-1}c^{n-1}}{2\Delta t} + \nabla\cdot(\mathbf{v}_s^{n+1}c^{n+1}\phi_s^{n+1}) = -g_c^{n+1} + \nabla\cdot(D_s\phi_s^{n+1}\nabla c^{n+1}). \tag{4.7}$$

The spatial discretization is done using central differences to ensure at least second order accuracy in space. The boundary conditions at the top and bottom boundaries $y = 1, 0$ are handled in the following way.

We use uniform mesh size in both spatial and temporal discretization, where the time step size is Δt and spatial mesh size is $\Delta x = L/M_x$, $\Delta y = 1/M_y$, $\Delta z = L_z/M_z$. The computation domain $\Omega = [0, L] \times [0, 1] \times [0, L_z]$ is divided into uniform cells by nodes $(x_i, y_j, z_k) = (i\Delta x, j\Delta y, k\Delta z)$, $i = 0, \cdots, M_x$, $j = 0, \cdots, M_y$, $k = 0, \cdot, M_z$. we denote the value of the numerical solution of (4.6) and (4.7) at $(n\Delta t, i\Delta x, j\Delta y, k\Delta z)$ by $\phi^n_{n,i,j,k}$, $c^n_{i,j,k}$ respectively. For either the case of the cavity geometry or the shear flow, we have $\mathbf{v} \cdot \mathbf{n}|_{0,1} = 0$. Thus the boundary condition for ϕ_n and c given by (2.12) and (2.13) becomes

$$\nabla c \cdot \mathbf{n}|_{y=0} = 0, \quad c|_{y=1} = c_1, \quad \nabla \phi_n \cdot \mathbf{n}|_{y=0,1} = 0, \quad \nabla \frac{\delta f}{\delta \phi_n} \cdot \mathbf{n}|_{y=0,1} = 0, \tag{4.8}$$

where c_1 is the dimensionless concentration at $y = 1$. The discrete forms of the boundary conditions (4.8) are given by

$$\phi^n_{n,i,1,k} = \phi^n_{n,i,-1,k}, \qquad \phi^n_{n,i,2,k} = \phi^n_{n,i,-2,k},$$
$$\phi^n_{n,i,M_y+1,k} = \phi^n_{n,i,M_y-1,k}, \qquad \phi^n_{n,i,M_y+2,k} = \phi^n_{n,i,M_y-2,k},$$
$$c^n_{i,1,k} = c^n_{i,-1,k}, \qquad c^n_{i,M_y,k} = c_1, \qquad i = 0, \cdots, M_x, \quad k = 0, \cdots, M_z. \tag{4.9}$$

The overall scheme is second order in space and first order in time formally. The density of solvent and polymer network are set to be the same in the calculations presented below, thus ρ^n is in fact a constant. The averaged Reynolds number Re_a is computed by

$$\frac{1}{Re_a} = \frac{\phi^n_{max}}{Re_n} + \frac{(1 - \phi^n_{max})}{Re_s},$$

where $\phi^n_{max} = \max\{\phi^n_{n,i,j}, 0 \le i \le M_x, 0 \le j \le M_y\}$. Thus Re_a is a constant at each time step t_n, but varies with time. We run the mesh refinement test for $\Delta x = \Delta y = \Delta z = 1/32$, $1/64$, $1/128$, $1/256$ respectively and the results show second order error reduction in space. Temporal mesh refine is done as well demonstrating a first order convergence rate in time. Thus our numerical scheme is convergent and stable upon mesh refinement. All numerical results presented here are for $\Delta x = \Delta y = \Delta z = 1/256$.

The projection steps are solved using Helmholtz and Poisson equation solver in FFT written in CUDA and the modified Cahn-Hilliard equation and the nutrient transport equation are solved using the BICGSTAB iterative method in CUDA on a CPU-GPU hybrid compute cluster.

5. Numerical Results and Discussions

We study dynamics of the biofilm-solvent interaction in two representative 3-D geometries: a shear cell with the periodic boundary condition for all physical variables in the x,

Table 1: Parameter values used in the simulation.

Symbol	Parameter	value	Unit
T	Temperature	303	Kelvin
γ_1	Distortional energy	8×10^6	$\text{kgm}^{-1}\text{s}^{-2}$
γ_2	Mixing free energy	3×10^{17}	$\text{kgm}^2\text{s}^{-2}$
χ	Flory-Huggins parameter	0.60	
λ	Mobility parameter	1×10^{-10}	$\text{kg}^{-1}\text{m}^3\text{s}$
N	Generalized polymerization parameter	1×10^3	
μ	Max. Production rate	1.4×10^{-4}	$\text{kgm}^{-3}\text{s}^{-1}$
k_c	Half saturation constant	1.5×10^{-4}	kgm^{-3}
k_1	Half saturation constant	1.5×10^{-4}	kgm^{-3}
A	Max. Consumption rate	0.1	$\text{kgm}^{-3}\text{s}^{-1}$
D_s	Substrate diffusion coefficient	2.3×10^{-9}	m^2s^{-1}
η_n	Dynamic viscosity of network	4.3×10^2	$\text{kgm}^{-1}\text{s}^{-1}$
η_s	Dynamic viscosity of solvent	1.002×10^{-3}	$\text{kgm}^{-1}\text{s}^{-1}$
ρ_n	Network density	1×10^3	kgm^{-3}
ρ_s	Solvent density	1×10^3	kgm^{-3}
c_0	Characteristic substrate concentration	1×10^{-3}	kgm^{-3}
h	Characteristic length scale	1×10^{-3}	m
t_0	Characteristic time scale	1×10^3	s
L_x, L_y, L_z	x, y, z-direction size of the computational domain Ω	1 or 4 $\times 10^{-3}$	m
M_x, M_y, M_z	number of sub-intervals in x, y, z-direction	256	

z-direction and the physical one in the y-direction. Table 1 lists the range of the dimensional parameter values used in our simulations.

In the simulations presented next, we first examine the growth of biofilms in a quiescent flow and their growth dynamics while coupled with the solvent flow; then, we simulate the deformation phenomenon in a shear cell in the weak flow regime. The interface between the biofilm and the surrounding water is distinguished by the level surface defined by $\Gamma = \{\mathbf{x} | \phi(\mathbf{x}, t) = 0^+\}$.

5.1. Growth dynamics of biofilms

The linearized stability of constant steady states of the model [28] revealed that the biofilm growth mechanisms are fueled by two possible sources. One is the mixing and the other is the growth of the EPS network and the bacterial population collectively. The stability analysis shows that a homogeneous biofilm is subject to a long wave instability leading to growth whenever the wave length of the 3-D biofilm colony exceeds a critical value due to mixing. This mechanism is the analogue of the gelation phenomenon in gels, where the small molecule solvent penetrates the effective polymer network to make the porus region bulge. In addition, the natural growth under the influence of the available nutrient in the solvent drives the growth across all wave length of the biofilm colony with a growth rate proportional to the local nutrient concentration.

In the 3-D simulations presented below, the no-flux boundary conditions are imposed

(a) $t = 0$

(b) $t = 100$

(c) $t = 200$

(d) $t = 300$
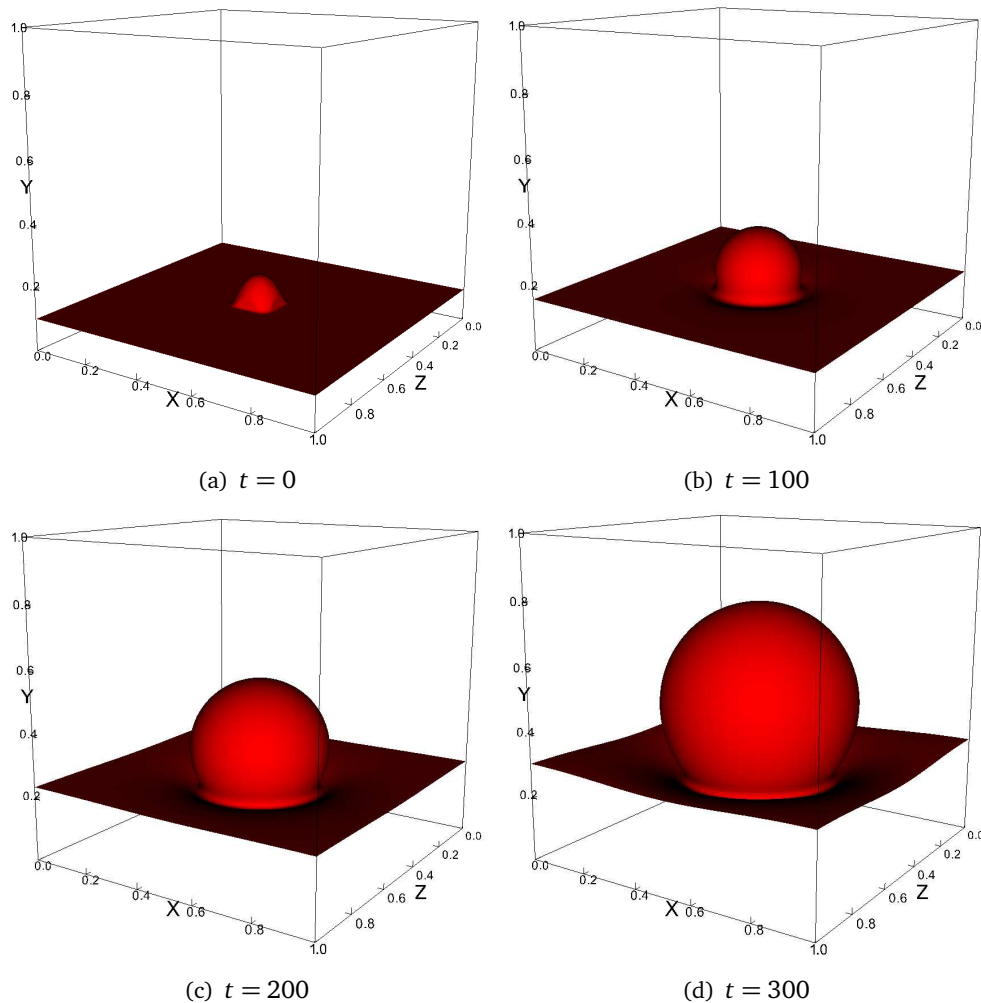
Figure 1: Single hump grows into a mushroom shaped colony in 3-D up to $t = 300$. The biofilm-solvent interface is defined by $\{\mathbf{x}|\lim_{\epsilon \to 0^+} \phi_n(\mathbf{x}, t) = \epsilon\}$.

for the polymer network volume fraction ϕ_n and the nutrient concentration c on all boundaries except that $c = c^\star$ is given at $y = 1$ (this is also known as the top feeding boundary condition). The velocities are assumed to be vanishing at all the solid boundaries while periodic in the x, z-directions. This setup mimics a fixed water container with nutrient being fed through the top boundary.

We first consider the scenario in which the initial distribution of the biofilm is uniform except for a single hump bulging up into the solvent region. The hump is located at the center of the biofilm-solvent interface in the chosen computational domain and eventually grows to a mushroom shape due to the accessibility to nutrients at the front is more readily than in the interior. This pattern of growth is often observed in biofilm growth. Here, our model captures it nicely. Fig. 1 plots the growth of the biofilm at a few selected time slots.

(a) $\mathbf{v}_n$ at $t = 200$

(b) $\mathbf{v}_s$ at $t = 200$

(c) $\mathbf{v}_n$ at $t = 300$

(d) $\mathbf{v}_s$ at $t = 300$
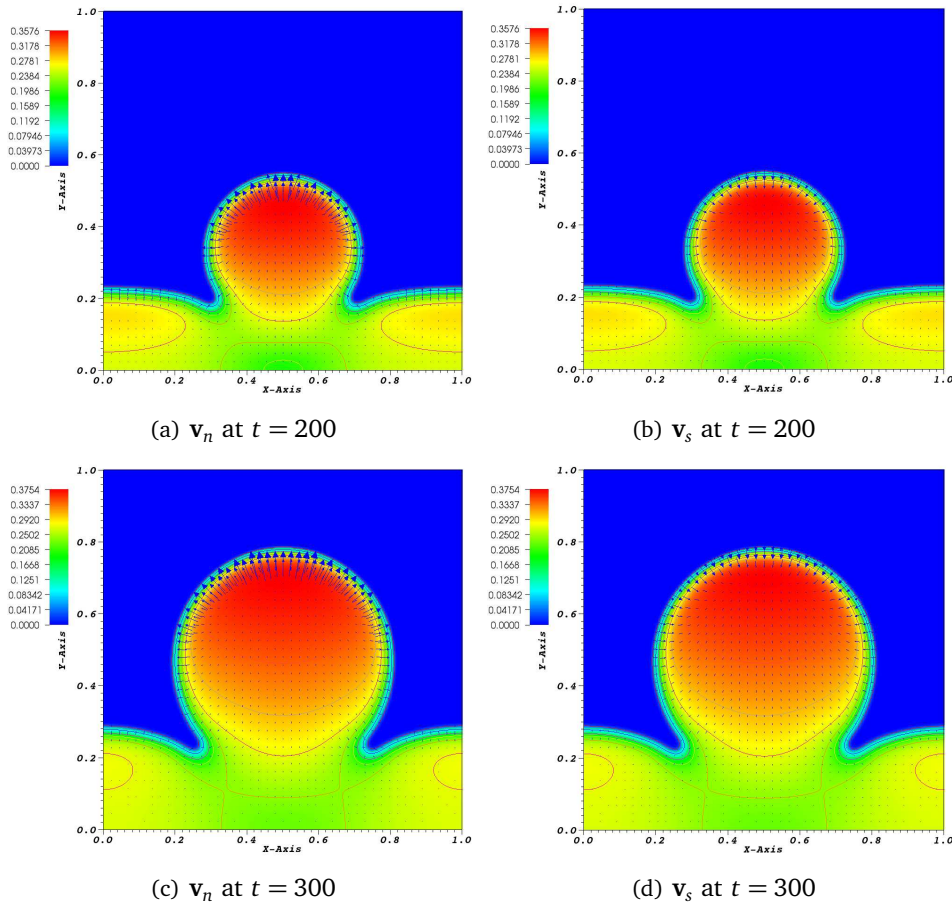
Figure 2: The cross-sectional biofilm profile along with the polymer and solvent velocity superimposed at $z = 0.5$ and $t = 200, 300$, respectively. The magnitude of the velocity is in the order of $O(10^{-4})$. So, the biofilm growth is a very slow process.

(a) $\mathbf{v}_n$ at $t = 300$

(b) $\mathbf{v}_s$ at $t = 300$
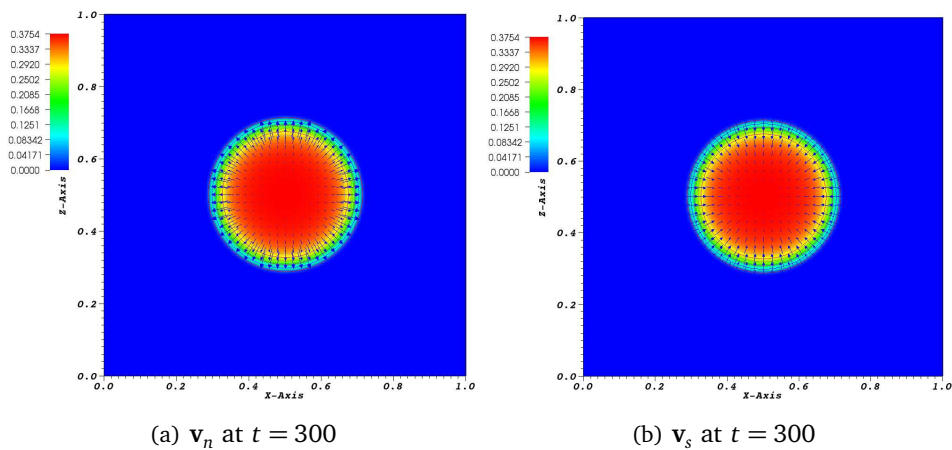
Figure 3: The cross-sectional biofilm profile and velocity field at $y = 0.7$ and $t = 300$. The velocity of the effective polymer as well as the effective solvent are superimposed on the biofilm density plot.

(a) $t = 0$

(b) $t = 70$

(c) $t = 140$

(d) $t = 210$
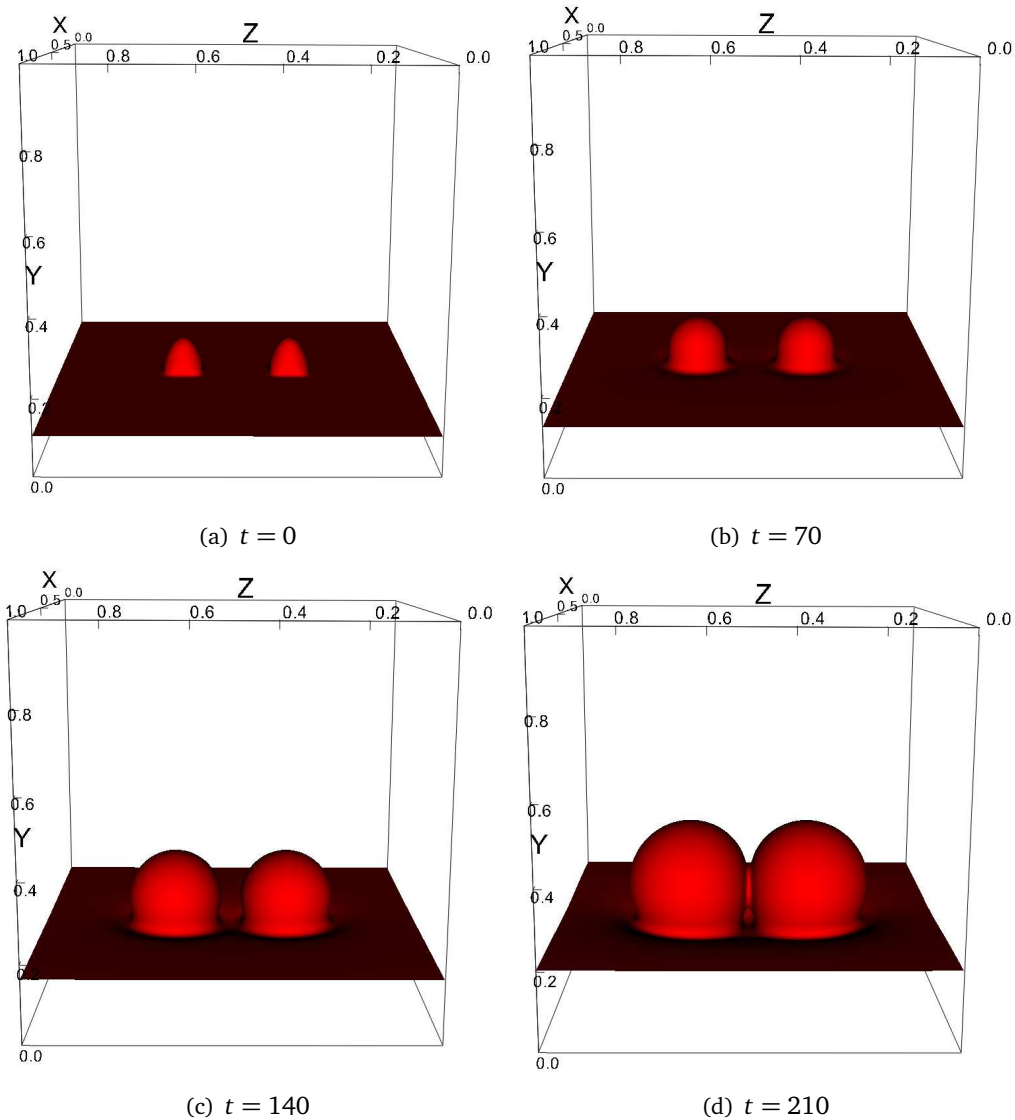
Figure 4: Growth of two nearby biofilm humps in 3-D up to $t = 210$. A bridge between the two colonies is formed in the later stage of the growth.

We note that the characteristic time scale is $t_0 = 1000$ seconds in the simulation, thus the dimensionless time $t = 300$ is approximately 3.5 days.

We plot a cross section of the computational domain at $z = 0.5$ to examine the detail of the growth dynamics in Fig. 2. We overlay the individual velocity for each component on top of the biofilm profile at $t = 200$ and $t = 300$, respectively. We notice that the polymer network velocity pointing outward at the biofilm-solvent interface while the solvent velocity pointing inward, indicating the growth of the biofilm is fueled by absorbing more solvent into the region, and expelling polymer outward pushing the expanding of the poly-

(a) $\mathbf{v}_n$ at $t = 210$ (b) $\mathbf{v}_s$ at $t = 210$
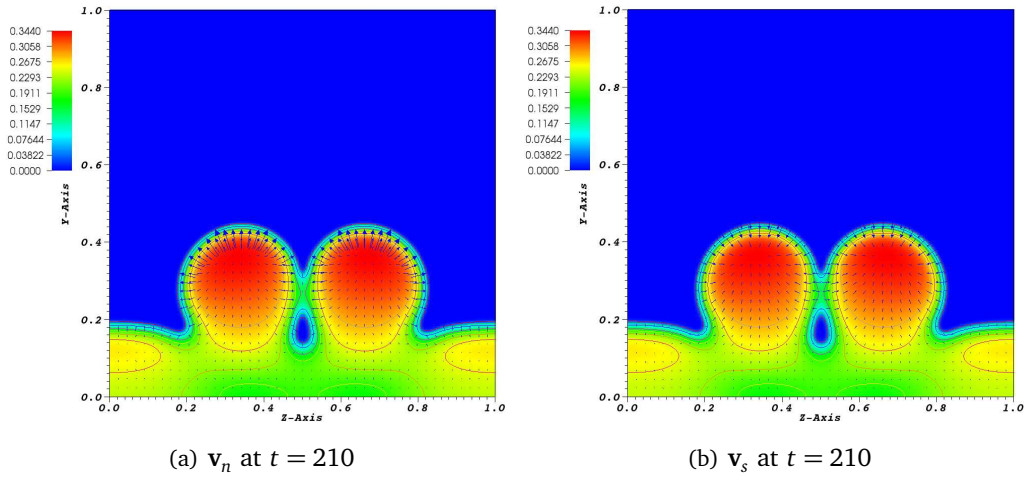
Figure 5: Cross-section of the biofilm profile and the superimposed velocity fields in y-z plane of two mushroom growth at $x = 0.5$ and $t = 210$.

(a) $\mathbf{v}_n$ at $t = 210$ (b) $\mathbf{v}_s$ at $t = 210$
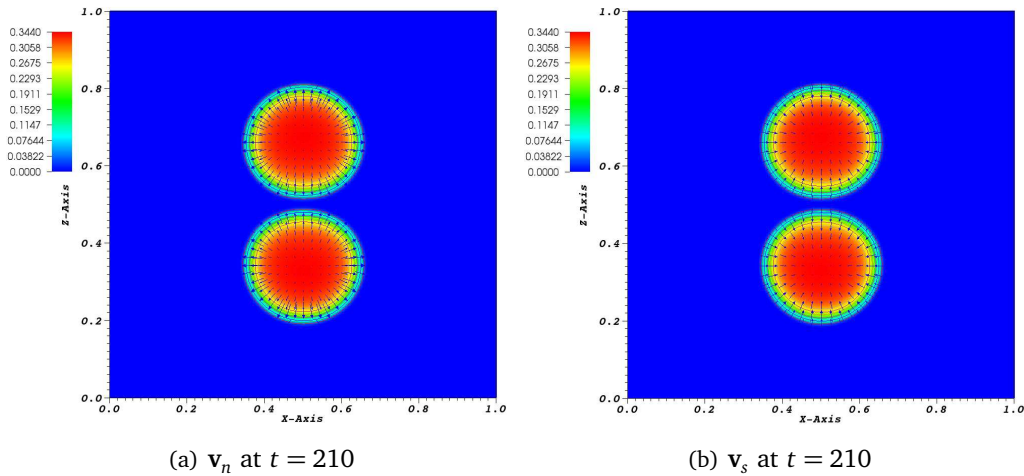
Figure 6: Cross-section of the biofilm profile and the superimposed velocity fields in x-z plane at $y = 0.35$ and $t = 210$.

mer network. Taking another cross section in the x-z plane at $y = 0.7$ shown in Fig. 3, this mutual exchange between the effective polymer and the solvent is shown more explicitly. The magnitudes of these velocities are weak though in the order of $O(10^{-4})$. But nevertheless, it illustrates the motion of each component during this slow dynamical process. We remark that the velocity field outside the biofilm is essentially the solvent velocity which is identical to the average velocity.

Water channels are quite common in biofilm colonies. We next look into the growth of two nearby humps to investigate the interaction between the growing mushroom islands and the formation of bridges between the mature mushroom shaped biofilm colonies and the water channel formed underneath. Fig. 4 depicts the 3-D biofilm profile for the growth

(a) $t = 0$

(b) $t = 50$

(c) $t = 100$

(d) $t = 150$
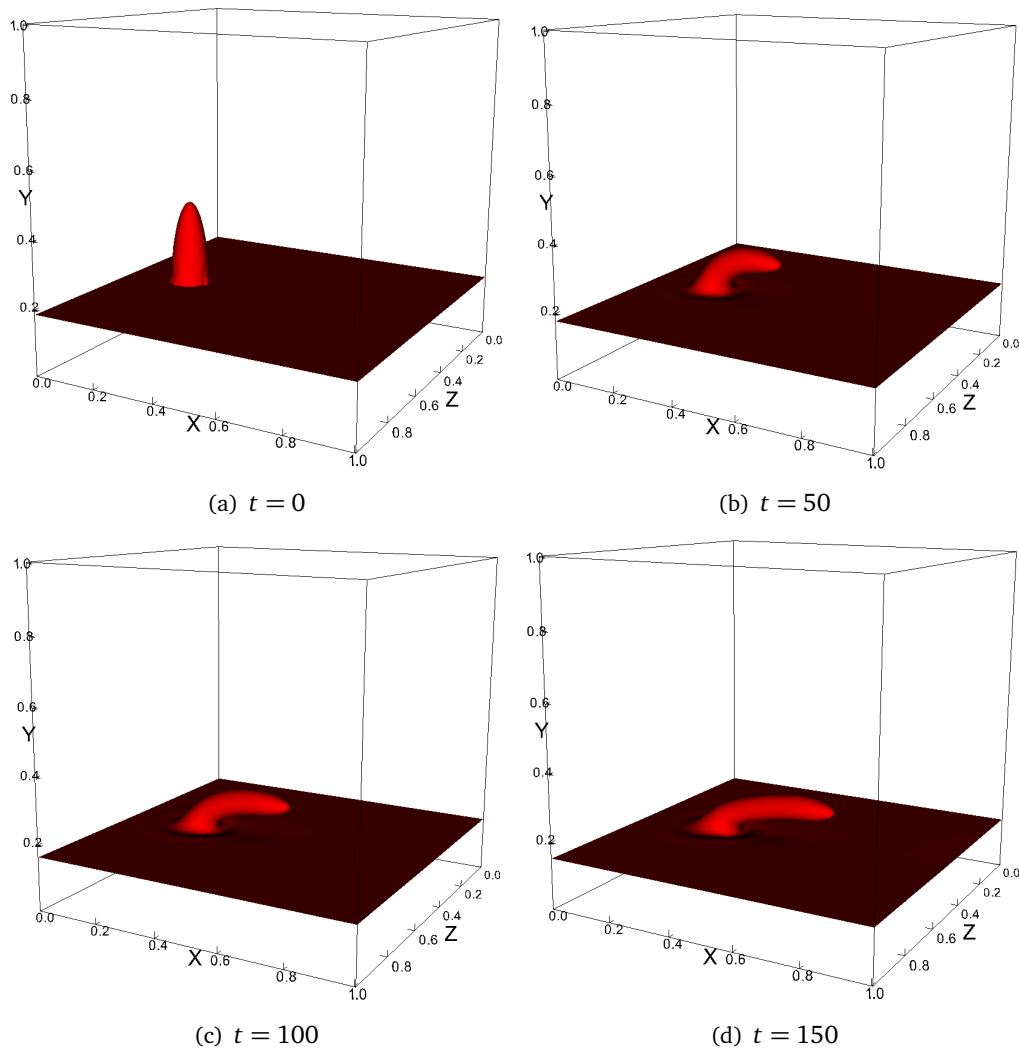
Figure 7: Single grown biofilm colony is sheared up to $t = 150$.

process from $t = 0$ to $t = 210$ when a bridge is firmly formed between the adjacent colonies. The 2-D slice views in Figs. 5 and 6 depict the polymer and solvent velocity field, respectively. The "exchange" between the two effective components are visible. In the water channel between the two colonies, the exchange is the weakest.

5.2. Biofilm in shear flows

We next examine how the ambient flow interact with a grown biofilm colony. We begin with a grown biofilm colony and then use the characteristic time scale $t_0 = 5s$ in the following computation for flow-biofilm interaction. The imposed boundary velocity is set at $v_x(x, 1, z, t) = 1$ (dimensionless). As expected the biofilm is dragged toward the flow

(a) $\mathbf{v}$ at $t = 150$

(b) $\mathbf{v}_n$ at $t = 150$

(c) $\mathbf{v}$ at $t = 150$

(d) $\mathbf{v}_s$ at $t = 150$
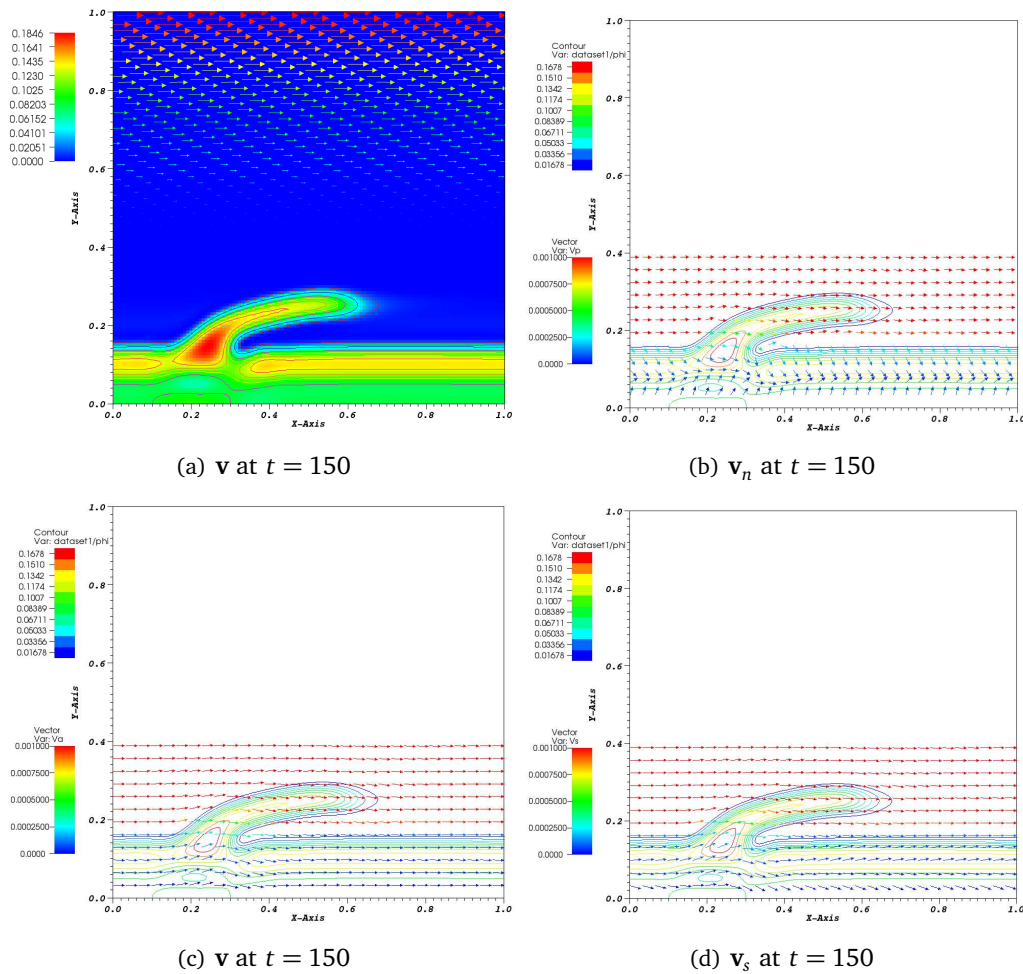
Figure 8: The biofilm profile along with the velocity fields at $z = 0.5$ and $t = 150$ in shear flows.

direction in the simulation. Thinning at the top of the colony is apparent. Fig. 7 depicts a few snapshots of the 3-D biofilm in the shear. Fig. 8 portraits the velocity fields at $t = 150$ in a cross section of the computational domain. In this case, the average velocity dominates and the excessive velocity for the polymer and solvent are much smaller in magnitudes. The flow field outside the biofilm exhibits a linear profile in the shear flow geometry. It is modified within the biofilm region though. The velocity for the effective polymer reveals a slight migration of the polymer component into the bulk biofilm region both from the water/biofilm interface and from the substrate. As a trade off water is squeezed away from the midsection of the bulk biofilm region into both the interface and the substrate. We have to warn the reader though that the magnitude of the velocities are so small that the migration is a weak phenomenon in the shear flow. Within the severely deformed peninsula region of the biofilm, the internal flow within the biofilm nearly coincide with the average velocity outside the biofilm.

6. Conclusion

We present some 3-D numerical simulations of the growth of biofilm colonies and their deformation in a water channel and under weak shear using the model we developed for biofilm and solvent mixtures recently [28]. The biofilm profile and the inter-mixing mechanism during the growth of biofilms are shown explicitly via velocity fields of each effective component. Grown biofilm colonies under shear exhibit significant stretching to the protruded biofilm colony due to the drag created by the shear flow. These results demonstrate the capability of the model and the numerical simulation tools developed based on it.

Acknowledgments

References

[1] A. N. Beris and B. Edwards, *Thermodynamics of Flowing Systems*, Oxford Science Publications, New York, 1994.

[2] R. B. Bird, R. C. Armstrong, O. Hassager, *Dynamics of Polymeric Liquids*, vol. 1 & 2, John Wiley and Sons, New York, 1987.

[3] J. W. Cahn and J. E. Hilliard, Free energy of a nonuniform system. I: interfacial free energy, J. Chem. Phys., 28 (1958), 258-267.

[4] J. W. Cahn, Free energy of a nonuniform system. II. Thermodynamic basis, J. Chem. Phys., 30(5) (1959), 1121-1124.

[5] J. W. Cahn and J. E. Hilliard, Free energy of a nonuniform system. III. Nucleation in a two-component incompressible fluid, J. Chem. Phys., 31 (1959), 688-699.

[6] N. Cogan and J Keener, The role of biofilm matrix in structural development, Math. Medicine Biol., 21(2) (2004),147-166.

[7] B. Costerton, Medical Biofilm Microbiology: The Role of Microbial Biofilms in Disease, Chronic Infections, and Medical Device Failure, CD-ROM, Montana State University, 2003.

[8] M. Doi and S. F. Edwards, *The Theory of Polymer Dynamics*, Oxford Science Publications, Oxford, 1986.

[9] M. Doi, *Introduction to Polymer Physics*, Oxford Science Publications, Oxford, 1995.

[10] P. J. Flory, *Principles of Polymer Chemistry*, Cornell University Press, Ithaca, NY, 1953.

[11] D. J. Hassett, P. A. Limbach, R. F. Hennigan, K. E. Klose, R. E. Hancock, M. D. Platt, D. F. Hunt, Bacterial biofilms of importance to medicine and bioterrorism: Proteomic techniques to identify novel vaccine components and drug targets, Expert Opin. Biol. Ther., 3(8) 2003, 1201-7.

[12] R. G. Larson, *The Rheology of Complex Fluids*, Oxford University Press, New York, 1998.

[13] C. A. A. Lima, R. Ribeiro, E. Foresti, M. Zaiat, Morphological study of biomass during the start-up period of a fixed-bed anaerobic reactor treating domestic sewage, Brazilian Arch. Biol. Tech., 48(5) (2005), 841-849.

[14] N. G. Cogan and J. Keener, Channel formation in gels, SIAM J. Appl. Math., 65(6) (2005), 1839-1854.

[15] I. Klapper, Effect of heterogeneous structure in mechanically unstressed biofilms on overall growth, Bull. Math. Biol., 66 (2004), 809-824.

[16] E. Alpkvist and I. Klapper, A multidimensional multispecies continuum model for heterogeneous biofilm development, Bull. Math. Biol., 69(2) (2007), 765-789.

[17] I Klapper, C. J. Rupp, R. Cargo, B. Purvedorj, P. Stoodley, Viscoelastic fluid description of bacterial biofilm material properties, Biotechnol. Bioeng., 80(3) (2002), 289-296.

[18] I. Klapper and J. Dockery, Role of cohesion in the material description of biofilms, Phys. Rev. E, 74 (2006), 031902.

[19] J. Dockery and I. Klapper, Finger formation in biofilm layers, SIAM J. Appl. Math., 62 (2002), 853-869.

[20] C. S. Laspidou and B. E. Rittmann, Modeling biofilm complexity by including active and inert biomass and extracelluar polymeric substances, Biofilm, 1 (2004), 285-291.

[21] C. Picioreanu, M. van Loosdrecht, J. Heijnen, Mathematical modeling of biofilm structure with a hybrid differential-discrete cellular automaton approach, Biotechnol. Bioeng., 58 (1998), 101-116.

[22] C. Picioreanu, M. van Loosdrecht, J. Heijnen, Multidimensional modelling of biofilm structure, Biotech. Microbial Biosystems: New Frontiers, Proceedings of the 8th International Symposium on Microbial Ecology, Bell CR, M. Brylinsky, P. Johnson-Green (eds), Atlantic Canada Society for Microbial Ecology, Halifax, Canada, 1999.

[23] C. Picioreanu, M. J-U Kreft, M. van Loosdrecht, Particle-based multidimensional multispecies biofilm models, Appl. Environ. Microbiol., May (2004), 3024-3040.

[24] C. Picioreanu, J. B. Xavier, M. van Loosdrecht, Advances in mathematical modeling of biofilm structure, Biofilm, 1 (2004), 337-349.

[25] J.-H. Pyo and J. Shen, Gauge-Uzawa methods for incompressible flows with variable density, J. Comp. Phys., 221 (2007), 181-197.

[26] H. Tanaka, Viscoelastic model of phase separation, Phys. Rev. E, 56(4) (1997), 4451-4462.

[27] C. Wolgemuth, E. Hoiczyk, D. Kaiser, G. Oster, How myxobacteria glide, Curr. Biol., 12 (2002), 369-377.

[28] T. Zhang, N. Cogan, Q. Wang, Phase-field models for biofilms. I. Theory and 1-D simulations, SIAM J. Appl. Math., 69(3) (2008), 641-669.

[29] T. Y. Zhang, N. Cogan, Q. Wang, Phase field models for biofilms. II. 2-D numerical simulations of biofilm-flow interaction, Commun. Comput. Phys., 4 (2008), 72-101.